Theoretical Study of the Adsorption and Decomposition of Sarin on Magnesium Oxide

A. Michalkova,[†,‡] M. Ilchenko,[‡] L. Gorb,[‡] and J. Leszczynski*[,‡]

Institute of Inorganic Chemistry, Slovak Academy of Sciences, Dúbravská Cesta 9, 842 36 Bratislava, Slovak Republic, and Computational Center for Molecular Structure and Interactions, Department of Chemistry, Jackson State University, 1400 Lynch Street, P.O. Box 17910, Jackson, Mississippi 39217

Received: September 16, 2003; In Final Form: February 3, 2004

The adsorption of Sarin (GB), isopropyl methylphosphonofluoridate ($C_4H_{10}FO_2P$), on the surface of magnesium oxide was investigated at the B3LYP/6-31G(d) and MP2/6-31G(d) levels of theory using the representative cluster models. The geometry of Sarin was fully optimized, while the geometry of the oxide fragment was kept frozen. The location and orientation of GB on the surface of MgO were found in cases when Sarin is physadsorbed or chemadsorbed. The adsorption results in the polarization and the electron density redistribution of GB. The interaction energies of Sarin−magnesium oxide corrected by the BSSE energy were predicted. The adsorption energy obtained at the MP2/6-31G(d) level of theory for the most stable chemadsorbed system is about −50 kcal/mol. The adsorption on the small fragment of MgO can lead to decomposition of Sarin.

1. Introduction

Sarin (GB), isopropyl methylphosphonofluoridate ($C_4H_{10}FO_2P$), is a very toxic organophosphorus compound. This substance became known as a nerve agent due to its effects on the disruption of nerve impulses in humans. This nerve agent is a lethal chemical warfare agent which was selected for its extreme and acute mammalian toxicity via inhalation or skin penetration.[1−3]

Metal oxides are well-known for their industrial applications as adsorbents, catalysts, and catalyst supports. Enhancement to the reactivity of nanosize oxides is anticipated due to the increased surface area, the greater amounts of highly reactive edge and corner "defect" sites, and unusual stabilized lattice planes.[4,5] The nanoparticles of MgO are unique. It was concluded that nanoparticles of MgO exhibit unusual surface morphologies and possess a more reactive surface.[4] Moreover, researchers found that nanocrystalline MgO, being 30% surface, can destroy organophosphorus compounds. MgO in a nanoparticle form has been successfully used as a destructive adsorbent for organophosphorus compounds.[6] The term "destructive adsorbent" is intended to describe its ability to efficiently adsorb and at the same time, to chemically destroy incoming adsorbate.

Within the last several years, important experimental studies of the fundamentals of the interactions between organophosphonate compounds and metal oxide surfaces have been carried out. Metal oxides such as MgO, Al_2O_3, FeO, CaO, TiO_2, α-Fe_2O_3, ZnO, and WO_3 are currently under consideration as destructive adsorbents for the decontamination of chemical warfare agents.[7,8] For example, several studies have investigated adsorption of dimethyl methylphosphonate (DMMP) (a widely used model compound for the simulation of interactions of phosphate esters with a surface) on the surface of these metal oxides.[9−22] In most of these works the authors have observed that, at first, DMMP adsorbed molecularly, via hydrogen bonding of the phosphoryl oxygen to a surface at an acid site, followed by stepwise elimination of the methoxy groups which combine with surface hydrogen atoms to yield methanol that evolves from the surface. The final product recorded for these oxides is a surface-bound methylphosphonate, with the P−CH_3 bond intact. On the basis of observations, it was concluded that not only are surface defect sites responsible for DMMP decomposition, but also Mg^{2+} and O^{2-} ions in the regular oxide surface take part in the process. In previous works[23−25] the authors, using solid-state MAS NMR, found that GB, Soman (GD − 3,3-dimethyl-2-butyl methylphosphonoflouridate ($C_7H_{16}FO_2P$)), VX (*O*-ethyl *S*-2-(diisopropylamino)ethyl methylphosphonothioate), and mustard (HD − bis(2-chloroethyl)sulfide) hydrolyze on the surface of the very reactive MgO, CaO, and Al_2O_3 nanoparticles. GD forms both GD−acid and methylphosphonic acid (MPA). VX and GD hydrolyze to yield surface-bound complexes of nontoxic ethyl methylphosphonate and pinacolyl methylphosphonate, respectively. Sarin undergoes initial molecular adsorption on aluminum oxide at unsaturated Al sites, followed by slow hydrolysis at room temperature.[26]

Since this paper is devoted to the study of adsorption of Sarin on the magnesium oxide surface, we will just mention that the pure surface of magnesium oxide has been a subject of many theoretical modeling studies (see, for example, reviews 27and 28, and works 29 and 30). To the best of our knowledge, there are no theoretical works concerning interactions between Sarin and metal oxides. Only several theoretical studies of the interactions between phosphate and clay minerals were published. These include the ONIOM study of adsorption of Sarin on dickite (a 1:1 dioctahedral mineral of the kaolinite group)[31] and theoretical studies of the interaction of phosphate with silica and hectorite published by Murashov and Leszczynski[32] and by Hartzell and co-workers.[33] GB will be adsorbed more preferably on the octahedral aluminum hydroxide surface than on the tetrahedral silica surface.[31] The ab initio calculations of hydrogen-bond complexes of dihydrogen and dimethyl phosphate anions with orthosilicic acid have shown that the phosphate groups can form strong hydrogen-bonded complexes with the silanols of the silica surface with stabilization energies of ca. −14 kcal/mol per hydrogen bond.[32] A molecular dynamic study of the large tributyl phosphate complex of europium provides a test of the sensitivity of force-field calculations to predict the behavior of molecules within the interlayer of a trioctahedral smectite clay−hectorite.[33]

Therefore, this work is intended to facilitate a more extensive understanding of the interactions of nerve agents with the surface

* Author to whom correspondence should be addressed. Phone: 001-601-9797824. Fax: 001-601-9797823. E-mail: jerzy@ccmsi.us.
† Slovak Academy of Sciences.
‡ Jackson State University.

10.1021/jp036766d CCC: $27.50
Published on Web 04/02/2004

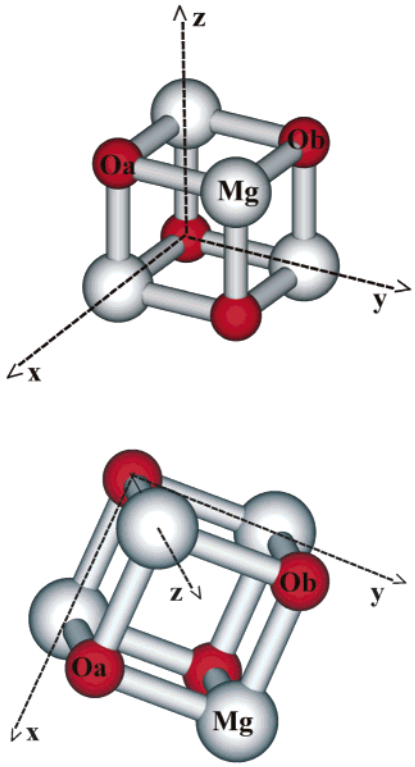

Figure 1. Mg_4O_4 fragment of MgO used to simulate the MgO surface. Two views of the cluster model in a starting geometry.

of nanoparticles of metal oxides that can lead to the development of techniques and remediation technologies for the decontamination of these compounds. It complements our recent study of the structures and properties of Sarin and Soman[34] and the adsorption of Sarin and Soman on dickite.[31] As the first example we have chosen the magnesium oxide which has a relatively simple crystal and surface structure. Therefore, it provides a good model for computational studies of its adsorption ability and reactivity.

2. Computational Details

The adsorption and decomposition of Sarin on the surface of magnesium oxide was investigated at the DFT level in conjunction with the B3LYP functional[35,36] and at the MP2 level of theory.[37−39] The 6-31G(d) basis set was used in both approximations. GB was allowed to fully relax. The geometry of the oxide fragment was kept frozen to the experimental bulk structure of a MgO crystal (the Mg−O bond lengths were set equal to 2.1 Å, and O−Mg−O bond angles were set at 90° and 180°). The simplest cubic part of this metal oxide contains four magnesium and four oxygen atoms (see Figure 1). We have prepared several cluster models of MgO since the cluster approximation is very effective for the study of the interaction of the surface of the solid material with the vicinity.

Two types of cluster models ("large" (L), this model mimics the adsorption on the regular part of nano-MgO (the size of nanoparticles falls between 2 and 10 nm, or 100−10000 atoms) and several types of "small" ones (S) which mimic adsorption on the irregular edges, corners, and defect sites) were used to simulate the surface of magnesium oxide. Since the calculation of models which contain more then 100 atoms are very time-consuming, the L model was prepared so that it consists of 16 magnesium and 16 oxygen atoms with a chemical formula of $Mg_{16}O_{16}$ (see Figure 2; this fragment is sufficient to model interactions of nanoparticles with Sarin since the surface of the

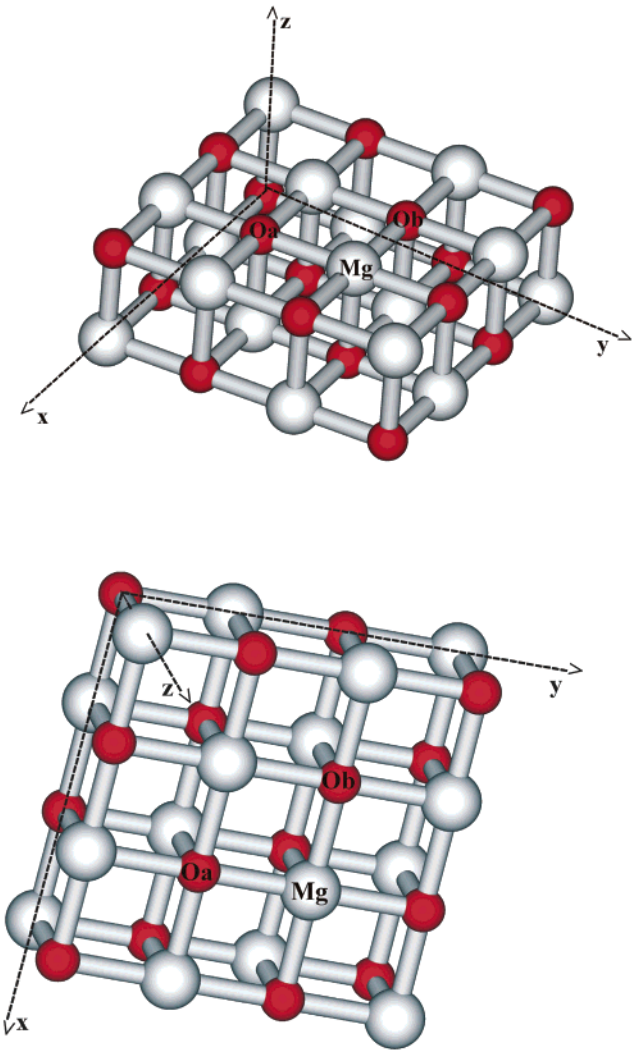

Figure 2. $Mg_{16}O_{16}$ fragment of MgO used to simulate the MgO surface. Two views of the cluster model in a starting geometry.

MgO fragment is much bigger than the molecule; the interactions with the border of the cluster are insignificant). The A1 small model contains four oxygen and magnesium atoms of magnesium oxide with a chemical formula of Mg_4O_4 (see Figure 1). The B and C small models simulate the hydroxylated surface of MgO. The B model, characterized by the $Mg_4O_4(OH)_2H_2$ formula, was constructed from the A model so that two hydroxyl groups were added to Mg atoms and two hydrogen atoms were added to the surface oxygen atoms of the MgO fragment. The C model ($Mg_4O_4(OH)H$) was selected from the basic A model so that one OH group was added to the Mg atom and one hydrogen atom was added to the surface oxygen atom of the A model. The hydroxylated B and C models are electroneutral. In the case of hydroxylated models, the whole organic fragment and attached hydroxyl groups and hydrogen atoms were optimized. All described models of MgO can be seen in Figures 3−7, which illustrate two views on the optimized structures of Sarin on the surface of MgO. For practical reasons we will use the R notation for the $-CH(CH_3)_2$ fragment of GB and the Oa and Ob notation for the surface oxygen atoms of the small models of MgO.

The interaction energy of the MgO−GB system corrected by the basis set superposition error (BSSE) was calculated. An analysis of the atomic charges of the studied MgO−GB system by fitting the electrostatic potential according to the ChelpG scheme[40] as implemented in the Gaussian98 program package[41]

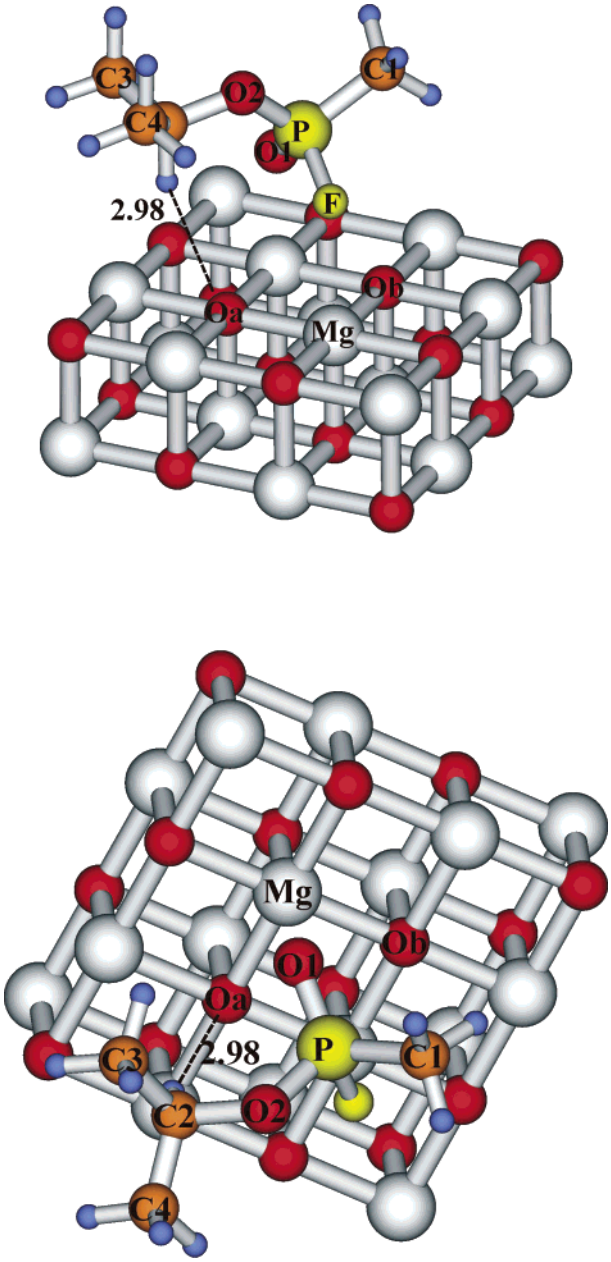

Figure 3. Magnesium oxide−Sarin adsorbed system: L−GB. Two views of the cluster model in an optimized geometry calculated at the B3LYP/6-31G(d) level.

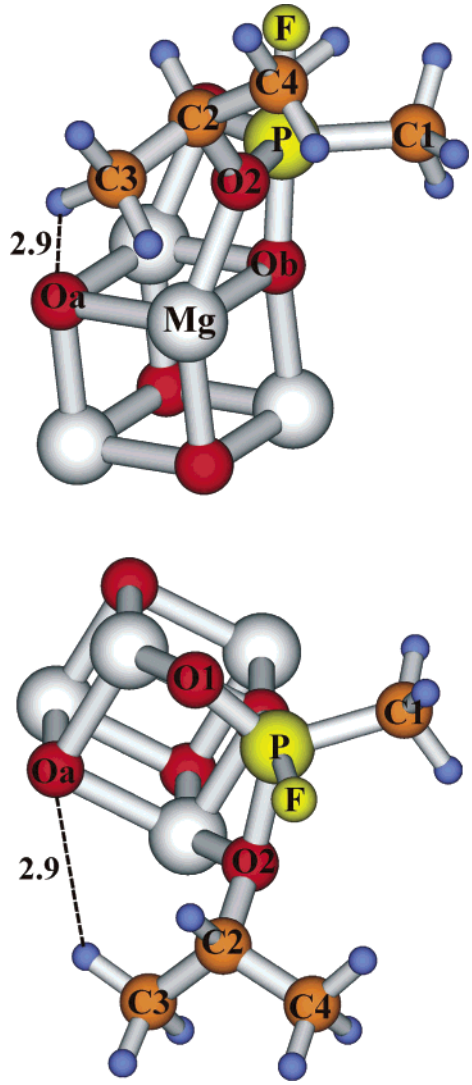

Figure 4. Magnesium oxide−Sarin adsorbed system: A1−GB. Two views of the cluster model in an optimized geometry calculated at the B3LYP/6-31G(d) level.

has been performed. The topological characteristics of electron density distribution following Bader's "Atoms in Molecules" theory[42] have been studied using the large model of MgO.

3. Results and Discussion

3.A. Adsorption on the Regular Nanosurface of MgO. At first, we performed the calculations of the adsorption of Sarin on the regular nanosurface of MgO using the L model. In this part we will discuss the structure, the interactions, and the interaction energy of this type of adsorption system. The optimized structure of Sarin on the MgO surface obtained using the large model of MgO at the B3LYP/6-31G(d) level of theory is displayed in Figure 3.

3.A.1. Structure and Intermolecular Interactions. One can see in Figure 3 that the position and orientation of adsorbed GB on the surfaces of MgO correspond to its ability to maximally locate on the surface of MgO. The O1 oxygen and fluorine atom are oriented directly toward the Mg atoms of the surface and the C2−H group to the oxygen atom of the surface.

The "atoms in molecules" (AIM) theory is the method that provides a rigorous and unambiguous criterion to determine which atoms are bonded in the system. Boyd and Choi[43,44] used the AIM theory to characterize hydrogen bonds from the charge density for a large set of acceptor molecules, involving HF and HCl as donors. This theory has provided new insights into conventional intermolecular hydrogen bonding.[45,46] Further, the AIM theory was applied to identify C−H···O contacts of DNA bases[47] and interaction of DNA bases with water.[48] The AIM analysis includes the location of the (3,−1) bond critical points on the surface of the total charge density, the analysis of the electron density (ρ), and the Laplacian of electron density ($\nabla^2\rho$) at the bond critical point, an analysis of the distances of formed bonds, and changes of electron density on atoms involved in the formation of the bonds. The existence of a bond critical point (3,−1) characterizes the formation of chemical bonds independently from its nature.[42]

Table 1 contains values of ρ and $\nabla^2\rho$ at the (3,−1) bond critical point and interatomic distances obtained at the B3LYP/6-31G(d) level. As follows from the AIM analysis, the formation of ion−dipole bonds between the O1 and F atoms of Sarin and Mg atoms of the MgO surface and dipole−dipole interactions

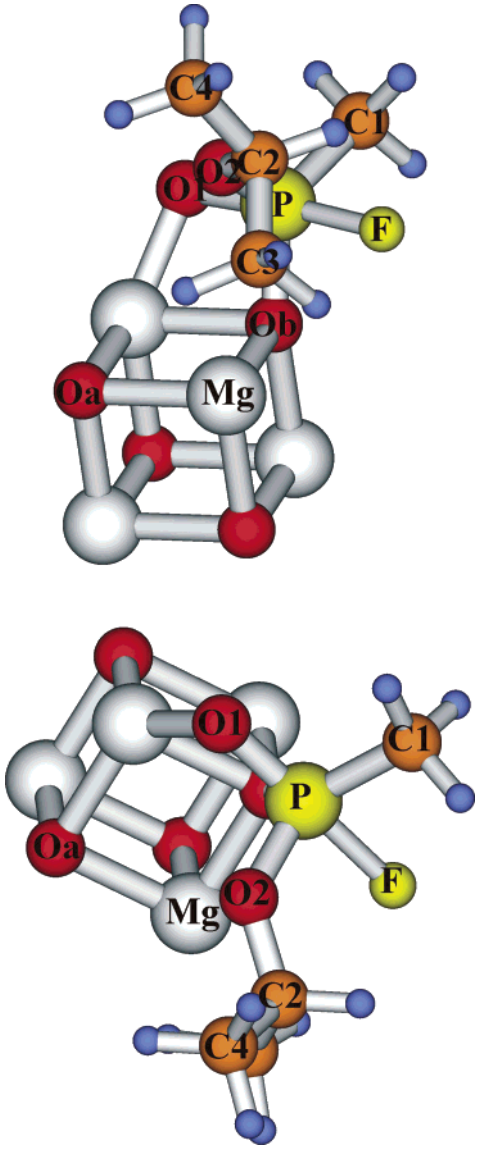

Figure 5. Magnesium oxide−Sarin adsorbed system with a different optimized structure of the adsorbed molecule: A2−GB. Two views of the cluster model in an optimized geometry calculated at the B3LYP/6-31G(d) level.

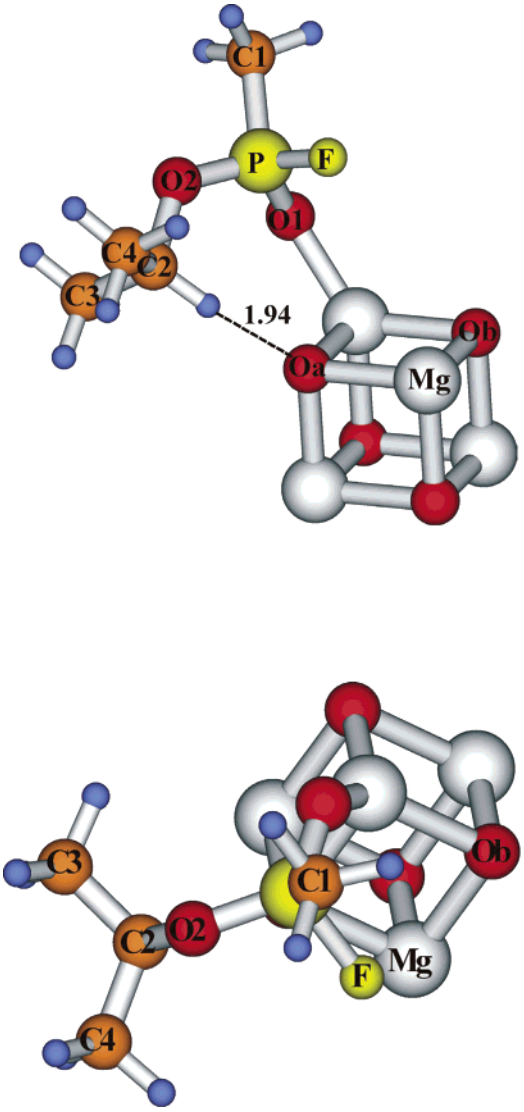

Figure 6. Magnesium oxide−Sarin adsorbed system with a different optimized structure of the adsorbed molecule: A3−GB. Two views of the cluster model in an optimized geometry calculated at the B3LYP/6-31G(d) level.

between the O1 and F atoms of Sarin and the Oa and Ob oxygen atoms of the surface is revealed. In the case of the Mg···F and Mg···O bonds, the values of ρ and $\nabla^2\rho$ are two and four times larger than for other bonds. These large values correspond to the shorter distance between interacting atoms (the Mg···O distance is 2.34 Å and the Mg···F distance is 2.53 Å). It indicates that these bonds provide the most stabilizing interactions in the studied adsorbed $Mg_{16}O_{16}$−GB system. Further, the AIM analysis reveals that the adsorption of GB on the surface of MgO occurs also due to the formation of the hydrogen bond between the C2−H group of Sarin and the Oa oxygen atom of the MgO surface with the 2.98 Å O···H distance. The values of ρ and $\nabla^2\rho$ characterizing this hydrogen bond are positive and range from 0.0048 au to 0.015 au.

The interaction energy corrected by the BSSE of the $MgO_{16}O_{16}$−GB adsorption system obtained at the B3LYP/6-31G(d) level is only −2.9 kcal/mol. Sarin interacts weakly with the MgO surface because of the formation of only one C−H···O hydrogen bond with a binding energy of only a fraction of a kcal/mol and weak ion−dipole interactions between the oxygen and fluorine atoms of Sarin and the MgO surface.

On the basis of values of interatomic distances and values of adsorption energies, one may conclude that due to the adsorption of Sarin on the regular nanosurface of MgO, a magnesium ion is involved in intermolecular interactions only through ion−dipole interactions. Magnesium does not create any strong chemical bond with the organic molecule. This is the reason Sarin is only physadsorbed (only weak interactions are formed between Sarin and the surface of MgO, the physical and chemical characteristics of Sarin are modified but they are not changed significantly) and weakly stabilized on such a surface type.

3.A.2. Changes in Geometry and Polarization of Sarin. Tables 2 and 3 contain geometrical parameters of adsorbed and isolated GB obtained at the B3LYP/6-31G(d) level using the large model. One can see that the formation of MgO−GB complexes results in changes in the gas-phase geometric characteristics and conformation of adsorbed Sarin. The physadsorption of GB on the regular nanosurface leads to insignificant changes in geometry. One can see that the bond lengths between heavy atoms of adsorbed GB are changed on average by about 5%. However, a comparison of angles and dihedral angles of adsorbed GB on the nanosurface and isolated GB reveals that

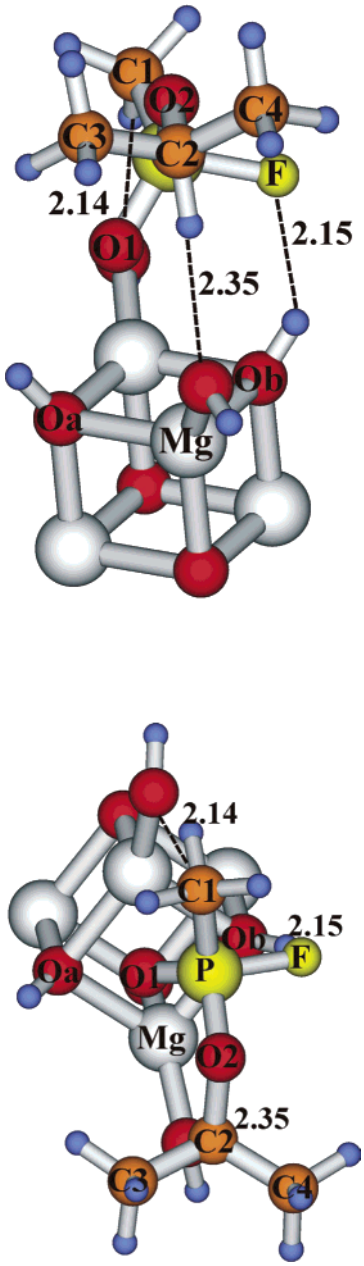

Figure 7. Hydroxylated magnesium oxide−Sarin adsorbed system: B−GB. Two views of the cluster model in an optimized geometry calculated at the B3LYP/6-31G(d) level.

TABLE 1: Electron Density ρ (au) and Laplacian of Electron Density $\nabla^2\rho$ (au) Values from the AIM Analysis and Distances D (Å) of Formed Bonds for the $Mg_{16}O_{16}$−GB System Calculated at the B3LYP/6-31G(d) Level of Theory

bond/ characteristic	ρ	$\nabla^2\rho$	D^a
C−H···Oa	0.0048	0.0150	2.98(156.9)
F···Mg	0.0085	0.0529	2.53
O···Mg	0.0162	0.0969	2.34
F···Oa	0.0076	0.0257	3.18
F···Ob	0.0083	0.0281	3.12
O1···Oa	0.0108	0.0291	3.09
O1···Ob	0.0106	0.0285	3.11

[a] C−H···Oa angle (in degrees) is in parentheses.

the MgO surface does not have a significant influence on changes of the conformation of GB.

The adsorption results in a redistribution of the electron density of GB, usually thought of as an internal polarization. Tables 4 and 5 contain atomic charges obtained using the

TABLE 2: Geometric Parameters[a] of Adsorbed and Isolated GB Obtained Using the B3LYP/6-31G(d) Method

system	A−GB	A−GB(f)	B−GB	C−GB	L−GB	GB
D(P−O1)	1.561	1.530	1.494	1.512	1.484	1.478
D(P−F)	1.678	3.612	1.612	1.587	1.617	1.600
D(P−O2)	1.776	1.611	1.587	1.558	1.593	1.604
D(P−C1)	1.838	1.807	1.788	1.796	1.800	1.804
D(C2−O2)	1.466	1.459	1.491	1.526	1.482	1.469
D(C2−C3)	1.526	1.522	1.520	1.517	1.521	1.524
D(C2−C4)	1.522	1.529	1.520	1.519	1.520	1.521
D(C1−H)[b]	1.093	1.097	1.096	1.093	1.093	1.093
D(C2−H)	1.090	1.097	1.096	1.104	1.095	1.095
D(C3−H)[b]	1.098	1.097	1.095	1.095	1.095	1.095
D(C4−H)[b]	1.095	1.095	1.095	1.096	1.095	1.095
α(O1−P−C1)	121.9	114.9	116.7	112.2	117.3	118.3
α(O1−P−O2)	120.3	108.8	115.2	119.0	117.0	117.0
α(O1−P−F)	94.5	119.7	109.4	108.4	112.8	112.4
α(P−O2−C2)	125.3	125.9	121.4	129.6	120.8	120.8
γ(O1−P−C1−O2)	179.1	123.6	131.1	130.6	130.9	130.2
γ(O1−P−F−O2)	120.2	−169.3	−123.1	−129.5	−126.3	−126.6
γ(F−P−C1−O2)	84.7	−126.1	−108.7	−112.3	−105.6	−106.1

[a] Bond lengths (D) are in Å ,and angles (α) and dihedral angles (γ) are in degrees. [b] Average value.

TABLE 3: Geometric Parameters[a] of Adsorbed and Isolated GB Obtained Using the MP2/6-31G(d) Method

system	A−GB	A−GB(f)	C−GB	GB
D(P−O1)	1.562	1.531	1.514	1.482
D(P−F)	1.679	3.618	1.589	1.602
D(P−O2)	1.763	1.622	1.563	1.607
D(P−C1)	1.823	1.791	1.784	1.791
D(C2−O2)	1.468	1.455	1.518	1.471
D(C2−C3)	1.519	1.529	1.510	1.515
D(C2−C4)	1.514	1.515	1.510	1.513
D(C1−H)[b]	1.091	1.093	1.091	1.091
D(C2−H)	1.089	1.096	1.101	1.096
D(C3−H)[b]	1.097	1.097	1.094	1.093
D(C4−H)[b]	1.093	1.093	1.094	1.093
α(O1−P−C1)	122.5	115.5	112.5	118.5
α(O1−P−O2)	120.6	108.6	119.1	117.3
α(O1−P−F)	94.4	117.9	108.5	112.3
α(P−O2−C2)	124.4	123.7	126.5	118.2
γ(O1−P−C1−O2)	179.2	123.4	130.6	130.5
γ(O1−P−F−O2)	120.4	−167.0	−126.3	−126.6
γ(F−P−C1−O2)	84.8	−128.3	−105.6	−105.6

[a] Bond lengths (D) are in Å, and angles (α) and dihedral angles (γ) are in degrees. [b] Average value.

TABLE 4: ChelpG Atomic Charges of Adsorbed and Isolated GB Obtained Using the B3LYP/6-31G(d) Method

system	A−GB	A−GB(f)	B−GB	C−GB	L−GB	GB
P	1.191	1.174	1.128	1.154	1.282	1.005
F	−0.340	−0.672	−0.283	−0.260	−0.374	−0.252
O1	−0.774	−0.690	−0.596	−0.704	−0.782	−0.600
C1	−0.367	−0.440	−0.514	−0.394	−0.424	−0.451
O2	−0.582	−0.535	−0.514	−0.559	−0.595	−0.499
C2	0.569	0.543	0.524	0.620	0.684	0.532
C3	−0.407	−0.239	−0.323	−0.273	−0.319	−0.326
C4	−0.289	−0.320	−0.405	−0.401	−0.288	−0.319
H[a](−C1)	0.101	0.153	0.178	0.134	0.133	0.146
H(−C2)	−0.017	−0.048	−0.085	0.007	−0.084	−0.021
H[a](−C3)	0.104	0.071	0.077	0.063	0.074	0.090
H[a](−C4)	0.065	0.088	0.100	0.107	0.066	0.084

[a] Average value.

ChelpG scheme of adsorbed and isolated Sarin at the B3LYP/6-31G(d) level. The charges of atoms involved in the interactions with the surface (F, O1, P, C2, and H(−C2)) are increased, while the charges of the C1, C3, and C4 atoms decrease (in absolute value). The changes of atomic charges in the adsorbed Sarin are relatively large. For example, the phosphorus charge changes by only 0.3 e for the L−GB model. These large changes are caused by the character of attractive interactions between Sarin and the surface.

The conclusion of this part of the study is that the adsorption of Sarin on the regular nanosurface of MgO could be character-

TABLE 5: ChelpG Atomic Charges of Adsorbed and Isolated GB Obtained Using the MP2/6-31G(d) Method

system	A−B	A−GB(f)	C−GB	GB
P	1.434	1.400	1.426	1.319
F	−0.413	−0.738	−0.323	−0.325
O1	−0.888	−0.796	−0.836	−0.732
C1	−0.421	−0.467	−0.497	−0.550
O2	−0.660	−0.616	−0.676	−0.618
C2	0.623	0.559	0.727	0.650
C3	−0.489	−0.298	−0.338	−0.377
C4	−0.328	−0.392	−0.444	−0.362
H[a](−C1)	0.110	0.156	0.154	0.163
H(−C2)	−0.007	−0.021	0.019	−0.043
H[a](−C3)	0.124	0.097	0.077	0.094
H[a](−C4)	0.074	0.111	0.115	0.087

[a] Average value.

ized as physadsorption (the interactions of Sarin with the nanoparticle of MgO do not lead to the decomposition of this molecule). Therefore, in the next section we present the results of the decomposition of Sarin using the simplest Mg_4O_4 cubic cell of MgO.

3.B. Adsorption on a Small Fragment of MgO. The optimized structures of Sarin on the MgO surface obtained using a small model at the B3LYP/6-31G(d) level are illustrated in Figures 4−6. Tables 2 and 3 contain geometric parameters of the A1−GB and C−GB studied models obtained at the B3LYP/6-31G(d) and MP2/6-31G(d) levels. We have found the same position, orientation, and interactions of Sarin with the MgO surface at both levels of theory with small differences in geometry parameters. For example, this maximum difference in the bond lengths is about 0.01 Å and in angles and dihedral angles is about 2°. Therefore, we conclude that the calculation at the B3LYP/6-31G(d) level is sufficient for the study of the adsorption and decomposition of Sarin on the MgO surface. Therefore, the B−GB model was calculated only at this level.

3.B.1. Structure and Intermolecular Interactions. The molecule is placed on the surface so that the P, O1, and O2 atoms are located above the oxygen and magnesium atoms of the surface. The O1−P−O2 plane of Sarin is parallel with the surface.

The calculation of the small model of MgO with a different initial position for GB (the A1−GB, A2−GB, and A3−GB models) reveals that GB could be adsorbed on the MgO surface in three different ways. All of them are presented in Figures 4−6, denoted the A1−GB, A2−GB, and A3−GB models. Sarin is adsorbed on the surface due to the formation of chemical bonds between the P, O1, and O2 atoms (the A1 model), or the P and O1 atoms (the A2 model), or only the O1 atom (the A3 model) and the MgO surface. The P−O bond lengths between the phosphorus atom of Sarin and the surface oxygen atom are about 1.6 Å, and the O−Mg bond lengths between the O1 or O2 oxygen atoms and the Mg atom of the surface are about 2.0 Å. These covalent bonds contribute mostly to the stabilization of Sarin on the MgO surface. The experimental studies[12,13] of IR spectra of interactions of DMMP with magnesium oxide also found that initial chemadsorption (in this kind of adsorption, the covalent or ionic bond is formed between interacting compounds, the physical and chemical properties of adsorbent and adsorbate are changed significantly) involved the Lewis acid Mg surface sites binding to the phosphoryl oxygen. The finding of strong interactions between Sarin and the MgO surface in the first step of decomposition is consistent with the results of experimental studies[11,15] and a cluster quantum chemical study[49] of DMMP adsorption on magnesium oxide nanoparticles.

According to the values of the interaction energies, the A1 model is the most stable. The difference in corrected interaction

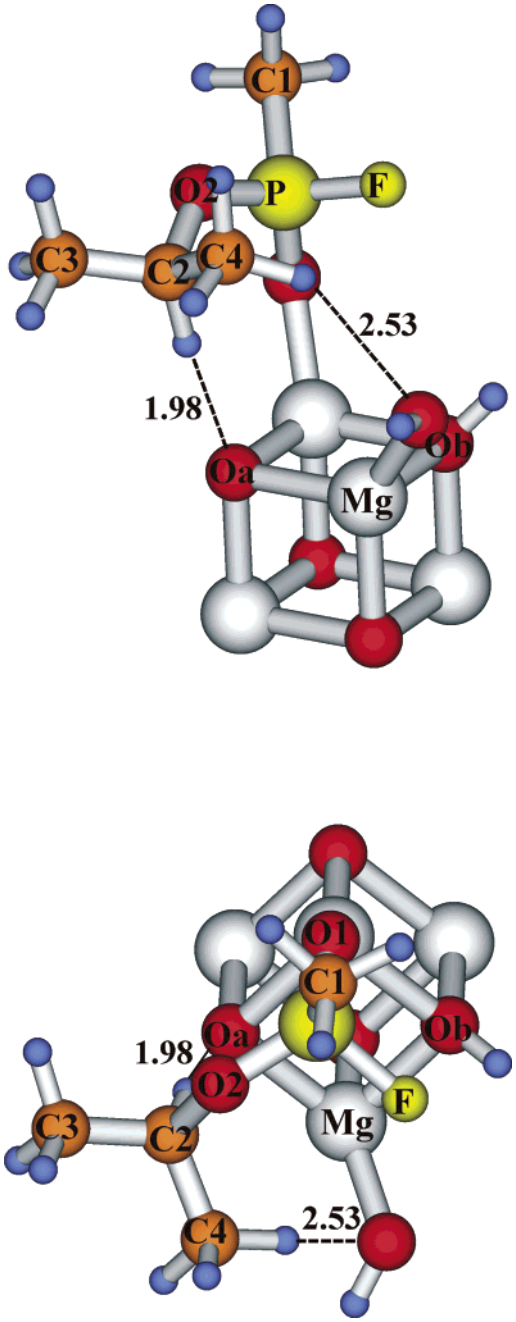

Figure 8. Hydroxylated magnesium oxide−Sarin adsorbed system: C−GB. Two views of the cluster model in an optimized geometry calculated at the B3LYP/6-31G(d) level.

energies is about 20 kcal/mol. It indicates that the formation of this type of complex with the formation of three covalent bonds despite the large change in conformation compared to the gas phase is the most advantageous. The interaction energies of these complexes with Sarin corrected by BSSE calculated at the B3LYP/6-31G(d) level of theory are much larger than the values of adsorption energy predicted using the large model. These large values confirm the chemadsorption of these species on the surface, which leads to the formation of the surface magnesium phosphonate complex. In the A1 model also the hydrogen bond between the C3−H group of Sarin as a proton-donor and the Ob oxygen atom of the MgO surface as a proton-acceptor provides a contribution to the interaction energy. The main difference in the interactions between Sarin and the MgO surface found using the A2 and A3 models comparing the discussed complex is in the number of covalent bonds. In the

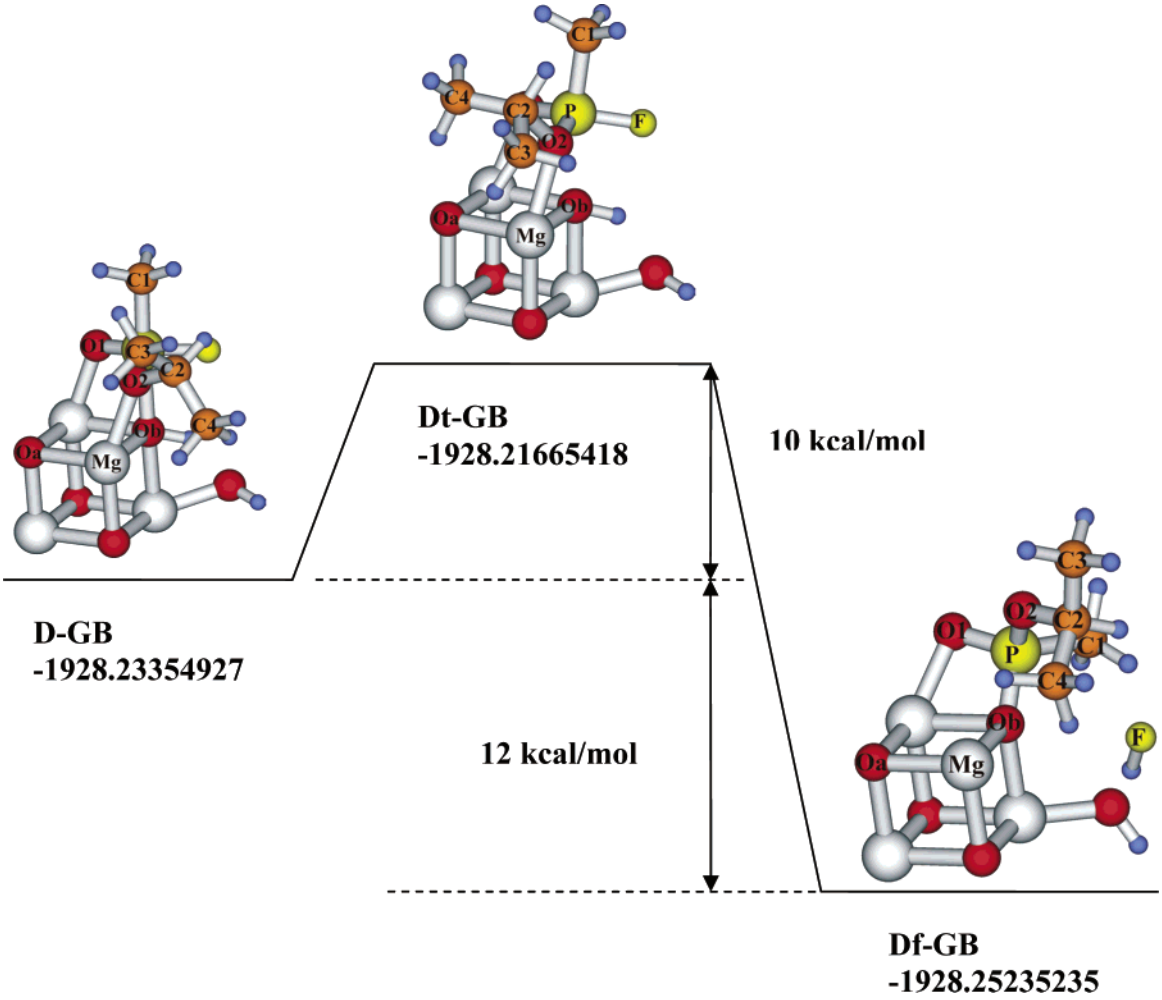

Figure 9. The scheme of transformation from the reactant (the D−GB model) through transition state (the Dt−GB model) into product (the Df−GB model) for the decomposition of Sarin on the hydroxylated MgO surface.

TABLE 6: BSSE-Corrected Interaction Energies (kcal/mol) of Studied Systems and Number of Covalent Bonds and O1−Mg Distance (Å) between Sarin and the Surface Calculated at the B3LYP/6-31G(d) and MP2/6-31G(d) Levels

system	A−GB		A1(f)−GB		B−GB	C−GB		L−GB
method	B3LYP	MP2	B3LYP	MP2	B3LYP	B3LYP	MP2	B3LYP
int. energy	−53.3	−50.2	−83.6	−53.4	−12.4	−39.3	−38.9	−2.9
no. of covalent bonds	3	3	3	3	0	1	1	0
O1−Mg distance (Å)	1.989	2.005	2.036	2.070	-	1.980	1.999	-

case of the A2 model, the O2 oxygen atom does not form a covalent bond with the surface. In the A3 model, only the O1 oxygen atom of Sarin forms a covalent bond (the bond length is 2.012 Å) with the magnesium atom of the surface. Moreover, the weak hydrogen bond between the C2−H group and the surface oxygen atom is created.

In addition to the described models, the small B and C models of hydroxylated MgO have been calculated (see Figures 7 and 8). In these models, the coordination of the surface oxygen is larger than in the nonhydroxylated model, and this reduces their reactivity, explaining the molecular physadsorption. Adsorbed Sarin is the most stable in the A1−GB model in comparison with the B−GB and C−GB models. Sarin is only physadsorbed on the surface of the B model so that the C1−H and C2−H groups form weak hydrogen bonds with the oxygen atoms of the hydroxyl groups of the MgO surface, and the fluorine atom forms one hydrogen bond with the surface OH group. The most stabilizing interactions in this case of adsorption are ion−dipole attractive interactions between the O1 oxygen atom of GB and the Mg atom of the MgO surface. In the C−GB model, one covalent bond between the O1 oxygen atom of Sarin and the Mg atom of the surface with a bond length of 1.98 Å and two weak C−H···O hydrogen bonds between the C2−H and C4−H bonds and oxygen atoms of the surface are formed. The values of interaction energies of the studied systems (the interaction energy was calculated as the difference between the total energy of the system and total energies of subsystems, see Table 6) are consistent with an increase in the number and strength of the formed covalent bonds between Sarin and the surface.

The L model has provided a different description of the process of adsorption of Sarin on the surface of MgO than was found using small cluster models of MgO. The difference could be caused by the larger reactivity of the surface of MgO in the case of the small cluster model. Such a surface is able to create stronger attractive contacts with the organic molecule. Therefore, the molecule on this type of surface can be better stabilized. It is in agreement with the experimental study of Klabunde et al.[4] where it has been demonstrated that properties of the adsorbed metal oxides depend on the particular size of particles.

The edge/corner location of an atom of a MgO fragment increases the surface reactivity of the small cluster. The electron density associated with such atoms changes through the forma-

tion of interactions with neighboring atoms in order to stabilize their positions. Therefore, in contrast to the adsorption on the regular surface, a magnesium ion of MgO plays a crucial role in the adsorption of the large organic molecule on the surface clusters mimicking highly reactive edges and corners of this oxide. When magnesium is involved in the intermolecular interactions through a chemical bond, the compound is chemadsorbed. Magnesium forms the strongest chemical bond with the O1 atom of Sarin in comparison with other chemical bonds between the molecule and the surface (see Table 6, model C−GB; the interaction energy corresponding to the Mg−O1 bond is about 40 kcal/mol).

3.B.2. Changes in Geometry and Polarization of Sarin. In the case of chemadsorption, the changes in geometric parameters are the greatest in the case of the A1−GB model for the O1, phosphorus, and C1 carbon atoms of Sarin. These changes correspond to the formation of covalent bonds with the surface of MgO. The P−O1 and P−F bonds of adsorbed GB are enlarged in comparison with isolated GB. The P−F bond is changed the most significantly (0.17 Å). The changes of the R part of adsorbed Sarin are insignificant (the R group is not involved in the interactions with the surface). The calculations at the B3LYP and MP2 levels show the same effect concerning the described changes of adsorbed Sarin. The physadsorption (the B−GB model of the hydroxylated MgO surface) leads to insignificant changes in geometry.

The polarization of Sarin caused by the formation of covalent bonds with the surface is much larger than the electron density transfer caused by the physadsorption. As one can expect, the more significant changes correspond with the P, O1, and F atoms of Sarin which are directly involved in the most stabilizing attractive interactions (the B−GB model) or the covalent bonds (other models) with the MgO surface. The calculations at the MP2 level result in larger values of atomic charges but with the same polarization trend as data obtained at the B3LYP level.

3.B.3. Modeling of the Decomposition of Sarin. The experimental studies[11,14,15] of interactions between DMMP and MgO nanoparticles reveal that if adsorption is strong enough, the adsorbate may be decomposed into fragments. They found that the methoxy group is removed from DMMP and the rest of DMMP reacts with the surface, forming adsorbed methyl methylphosphonate. Hypothetically, the application of this mechanism of decomposition of DMMP on the MgO surface for GB shows that GB should be adsorbed on the surface so that the P atom strongly interacts with the O atom of the surface (with the O atom of the hydroxyl group in the case of the hydroxylated MgO surface) and the O1 atom interacts with the Mg atom of the surface. Further, the fluorine atom should be removed from Sarin, and the fluorine atom creates the HF molecule with the H atom of the hydroxyl group of the surface (the hydroxylated MgO surface).

We have evaluated experimentally predicted decomposition of Sarin on the hydroxylated surface of MgO using the D−GB model. In this model the phosphorus atom forms a chemical bond with the hydroxylated oxygen atom of the surface and the O1 and O2 atoms form chemical bonds with the magnesium atoms. The optimized structure of this model is illustrated in Figure 9. The decomposition was initiated by a transfer of the hydrogen atom of the surface OH group to the central position between the oxygen atom of the surface and the fluorine atom of Sarin (the model Df−GB). The optimization results in the formation of the HF molecule. This system with HF is much more stable than the D−GB model. The difference in total energies is about 12 kcal/mol. Following the mechanism of the decomposition, we suggest that the strongly electronegative fluorine affects the hydrogen atom of the hydroxyl group so that this atom is transferred into the binding distance and forms a covalent bond with the fluorine atom. Then the bond between the fluorine atom and the phosphorus atom is broken, and the HF molecule is formed. HF is positioned in such a way that the hydrogen atom is oriented toward the oxygen atom of the surface hydroxyl group, and the fluorine atom is in the center between the C1 and C4 atoms. We have located the transition state for this reaction pathway (Dt−GB). The reaction pathway and the optimized structures of reactant (D−GB model), transition state (Dt−GB model), and product (Df−GB) and the total energies are illustrated in Figure 9. The structure of the transition state is such that the hydrogen atom remains chemically bonded to the oxygen atom of the surface. The value of the activation energy is about 10 kcal/mol. It means that this reaction pathway is realistic, and the proposed mechanism is in agreement with experimentally investigated decomposition of DMMP on the hydroxylated MgO surface.

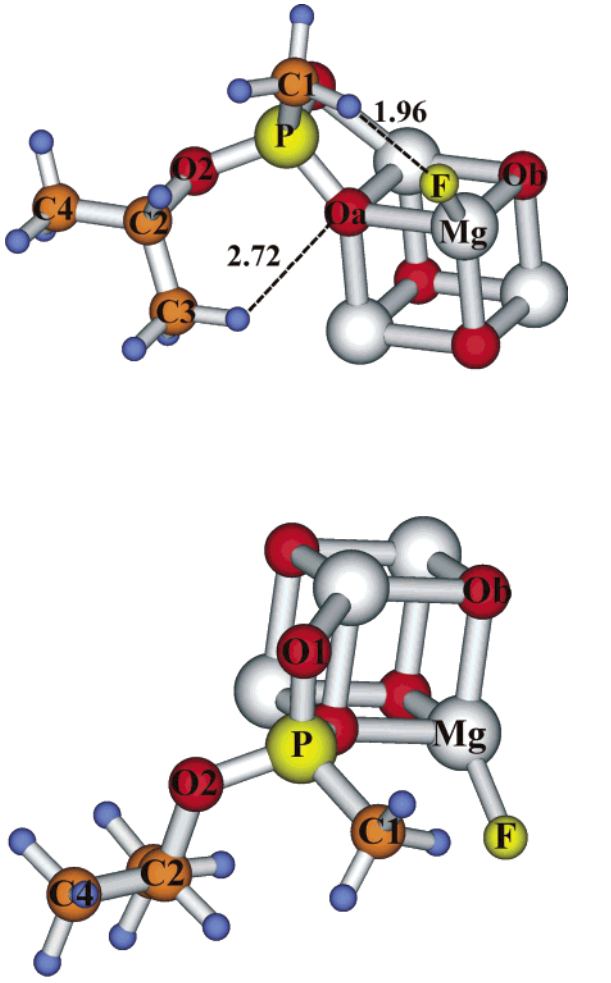

Figure 10. Two views of the optimized structure of decomposed Sarin on the MgO surface with fluorine transferred from Sarin into the binding distance with the Mg atom of the surface.

The decomposition of Sarin on the unhydroxylated surface of MgO was modeled. Using the A1 model, the removal of a fluorine from Sarin was modeled so that the fluorine atom was transferred from Sarin into binding distance with the Mg atom of the MgO surface (the A1(f)−GB model). The structure of decomposed Sarin on the MgO surface obtained using the A1-(f)−GB model at B3LYP/6-31G(d) level of theory is illustrated in Figure 10.

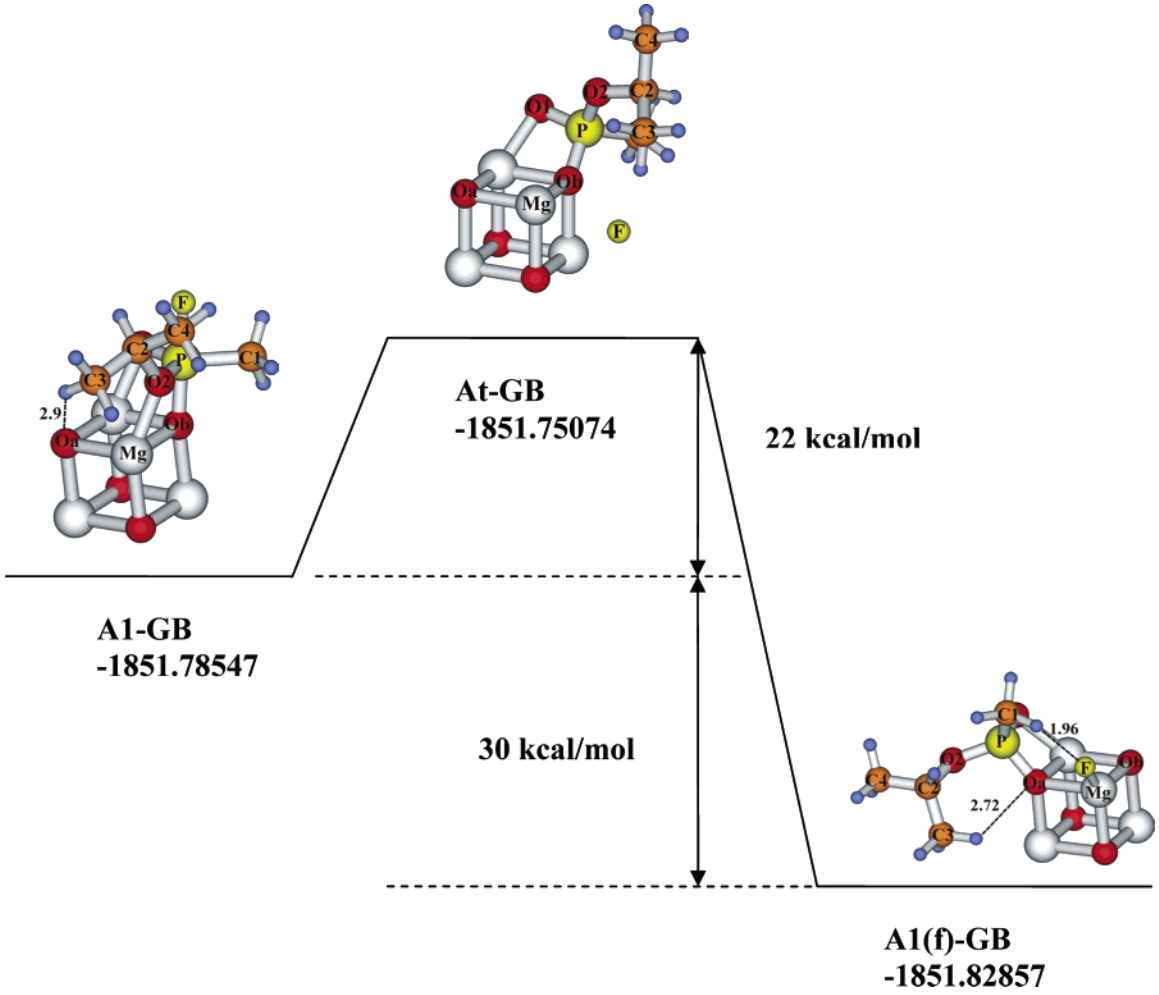

Figure 11. The scheme of transformation from the reactant (the A1−GB model) through transition state (the At−GB model) into product (the A1(f)−GB model) for the decomposition of Sarin on the unhydroxylated MgO surface.

The optimization of this model reveals that such a structure is realistic. In this system, Sarin interacts with the MgO surface so that the phosphorus atom and oxygen atom form covalent bonds with the Mg and Oa atoms of the surface; the C1−H group forms a hydrogen bond with the removed fluorine; and the C3−H group of Sarin forms a hydrogen bond with the Oa oxygen atom of the surface. The total energy of the A1(f) system calculated at the B3LYP/6-31G(d) level is about 30 kcal/mol larger than the total energy of the A1−GB model. It corresponds to the shorter P−Oa bond length (1.599 Å) between the phosphorus and oxygen atoms of Sarin and the surface atoms. The energy lost by the breaking of the P−F bond of Sarin is compensated by the interaction of the fluorine atom with the Mg atom of the MgO surface. A comparison of the geometry parameters of adsorbed Sarin in the A1−GB, A2−GB, and A1-(f)−GB adsorbed models with isolated Sarin reveals that the conformation of Sarin with a removed fluorine atom is more stable (the dihedral angles are very similar).

The calculation of the transition state of a fluorine transferring reaction from Sarin to the Mg atom was performed. The total scheme of the transformation from the reactant (the A1−GB model) through transition state (the At−GB model) to the product (the A1(f)−GB model) is presented in Figure 11 with values of total energies and differences between total energies of considered species. The structure of the transition state is such that the fluorine anion is placed against the center of the Mg_2O_2 square. The fluorine is almost in the middle of the transfer path from the position which it had in the A1−GB model to the final position in the A1(f)−GB model. A two-step reaction mechanism is assumed with the A1−GB model as a reactant: in the first step Sarin creates a stable adsorbed complex with MgO so that the P and O1 atoms form chemical bonds with the surface and the Mg−O2 covalent bond is created. However, the structure destabilizes this type of adsorption complex. We expect that the transfer of the fluorine atom to the surface of MgO is accompanied by a change in the conformation of Sarin. Therefore, in the second step the bond between P and F is broken; the fluorine atom is transferred to the Mg atom of the surface and the rest of Sarin adopts the most energetically favorable conformation. This orientation stabilizes the structure by means of the formation of a new Mg−F chemical bond with a 1.805 Å bond length. This reaction can be viewed to be a result of the competition between the acid Mg center on the surface and the phosphorus atom of Sarin. The probability of such a reaction pathway was determined by the calculation of the activation energy from the difference of total energies of the A1−GB and At−GB models. The value of the activation energy estimated from this comparison is about 22 kcal/mol (see Figure 11). The reasonable size of the activation barrier suggests that the proposed mechanism for the decomposition of Sarin is realistic.

4. Conclusions

The adsorption and decomposition of Sarin on the surface of magnesium oxide was studied using small and large models of

the MgO cluster at the B3LYP/6-31G(d) and MP2/6-31G(d) levels of theory.

A number of locations and orientations of Sarin on the regular nanosurface and on the small fragment of MgO were found. Sarin can be physadsorbed on the MgO surface (the nanosurface and hydroxylated small fragment; this is the undestructive adsorption) or chemadsorbed in the case of an unhydroxylated small fragment of MgO: destructive adsorption. The physadsorption of GB on the surface of MgO occurs due to the formation of hydrogen bonds and ion−dipole and dipole−dipole interactions between adsorbed GB and the surface. The chemadsorption occurs due to the formation of covalent bonds between the molecule and the surface.

The changes in the geometrical parameters of adsorbed Sarin, polarization, and electron density transfer are more significant in the case of chemadsorbed Sarin compared to changes in physadsorbed Sarin. Sarin adsorbed on the nanosurface or hydroxylated small fragment of MgO is much less stabilized than Sarin adsorbed on the nonhydroxylated small fragment of MgO. The interaction energy of Sarin adsorption systems on MgO is proportional to the number and strength of formed covalent bonds between Sarin and the surface.

The adsorption on the unhydroxylated small fragment of MgO can lead to decomposition of Sarin so that the fluorine atom is removed from Sarin and transferred into the binding distance with the Mg atom of the surface. Sarin on the hydroxylated small fragment of MgO can be decomposed by a process that yields the formation of the HF molecule.

Acknowledgment. This work was facilitated by the support of the Office of Naval Research Grant No. N00034-03-1-0116 and by the support of the Army High Performance Computing Research Center under the auspices of the Department of the Army Grant No. DAAD19-01-2-0014, Army Research Laboratory Cooperative agreement number DAAH04-95-2-0003/ contract number DAAH04-95-C-0008, the content of which does not necessarily reflect the position or the policy of the government, and no official endorsement should be inferred.

References and Notes

(1) National Policy Agency. White Paper on Police; Government of Japan: Tokyo, 1994−1995.
(2) http://www.defenselink.mil/news/Aug2002/b08132002_bt419−02.html.
(3) Yang Y.-C. *Acc. Chem. Res.* **1999**, *32*, 109.
(4) Klabunde, K. J.; Stark, J.; Koper, O.; Mohs, C.; Park, D. G.; Decker, S.; Jiang, Y.; Lagadic, I.; Zhang, D. *J. Phys. Chem.* **1996**, *100*, 12142.
(5) Stark, J. V.; Park, D. G.; Lagadic, I.; Klabunde, K. J. *Chem. Mater*. **1996**, *8*, 1904.
(6) Koper, O.; Li, Y. X.; Klabunde, K. J. *Chem. Mater.* **1993**, *5*, 500.
(7) Yang, Y.-C.; Baker, J. A.; Ward, J. R. *Chem. Rev.* **1992**, *92*, 1729.
(8) Yang, Y.-C. *Chem. Ind.* **1995**, 334.
(9) Templeton, M. K.; Weinberg, W. H. *J. Am. Chem. Soc*. **1985**, *107*, 97.
(10) Templeton, M. K.; Weinberg, W. H. *J. Am. Chem. Soc*. **1985**, *107*, 774.
(11) Li, Y.-X.; Klabunde, K. J. *Langmuir* **1991**, *7*, 1388.
(12) Li, Y.-X.; Schlup, J. R.; Klabunde, K. J. *Langmuir* **1991**, *7*, 1394.
(13) Lin, S.-T.; Klabunde, K. J. *Langmuir* **1985**, *1*, 600.
(14) Atteya, M.; Klabunde, K. J. *J. Chem. Mater*. **1991**, *3*, 182.
(15) Li, Y.-X.; Koper, O.; Atteya, M.; Klabunde, K. J. *J. Chem. Mater*. **1992**, *4*, 323.
(16) Henderson, M. A.; Jin, T.; White, J. M. *J. Phys. Chem*. **1986**, *90*, 4607.
(17) Aurian-Blajeni, B.; Boucher, M. M. *Langmuir* **1989**, *5*, 170.
(18) Mitchell, M. B.; Sheinker, V. N.; Mintz, E. A. *J. Phys. Chem. B* **1997**, *101*, 11192.
(19) Sheinker, V. N.; Mitchell, M. B *Chem. Matter*. **2002**, *14*, 1257.
(20) Mitchell, M. B.; Sheinker, V. N.; Tesfamichael, A. B.; Gatimu, E. N.; Nunley, M. J. *Phys. Chem. B* **2003**, *107*, 580.
(21) Kanan, S. M.; Tripp, C. P. *Langmuir* **2001**, *17*, 2213.
(22) Kanan, S. M.; Lu, Z.; Tripp, C. P. *J. Phys. Chem. B.* **2002**, *106*, 9576.
(23) Wagner, G. W.; Bartram, P. W.; Koper, O.; Klabunde, K. J. *J. Phys. Chem. B* **1999**, *103*, 3225.
(24) Wagner, G. W.; Bartram, P. W.; Koper, O.; Klabunde, K. *Phys. Chem. B* **2000**, *104*, 5118.
(25) Wagner, G. W.; Procell, L. R.; O'Connor, R. J.; Munavalli, S.; Carnes, C. L.; Kapoor, P. N., Klabunde, K. J. *J. Am. Chem. Soc*. **2001**, *123*, 1636.
(26) Kuiper, A. E. T.; van Bokhoven, J. J. G.; Medena J. *J. Catal*. **1976**, *43*, 154.
(27) Sauer, J.; Ugliengo, P.; Garrone, E.; Saunders, V. R. *Chem. Rev*. **1994**, *94*, 2095.
(28) Pacchioni, G. *Surf. Rev. Lett.* **2000**, *7*, 277.
(29) Sushko, P. V.; Shluger, A. L.; Catlow, C. R. A. *Surf. Sci.* **2000**, *450*, 153.
(30) Pacchioni, G. *Solid Surf. Sci*. **2000**, *2*, 161.
(31) Michalkova, A.; Gorb, L.; Ilchenko, M.; Zhikol, O. A.; Shishkin, O. V.; Leszczynski, J. *J. Phys. Chem. B* **2004**, *108*, 1918.
(32) Murashov, V. V.; Leszczynski, J. *J. Phys. Chem. A* **1999**, *103*, 1228.
(33) Hartzell, C. J.; Cygan, R. T.; Nagy, K. L. *J. Phys. Chem. A* **1998**, *102* (34), 6722.
(34) Kaczmarek, A.; Gorb, L.; Sadlej, A. J.; Leszczynski, J. *Struct. Chem.*, in press.
(35) Becke, D. J. *Chem. Phys.* **1993**, *98*, 5648.
(36) Yang, Lee W.; Parr, R. G. *Phys. Rev. B* **1998**, *B37*, 785.
(37) Head-Gordon, M.; Pople, J. A.; Frisch, M. J. *Chem. Phys. Lett*. **1988**, *153*, 503.
(38) Frisch, M. J.; Head-Gordon, M.; Pople, J. A. *Chem. Phys. Lett*. **1990**, *166*, 275.
(39) Frisch, M. J.; Head-Gordon, M.; Pople, J. A. *Chem. Phys. Lett*. **1990**, *166*, 281.
(40) Breneman, C. M.; Wiberg, K. B. *J. Comput. Chem.* **1990**, *11*, 361.
(41) Frisch, M. J.; Trucks, G. W.; Schlegel, H. B.; Scuseria, G. E.; Robb, M. A.; Cheeseman, J. R.; Zakrzewski, V. G.; Montgomery, J. A., Jr.; Stratmann, R. E.; Burant, J. C.; Dapprich, S.; Millam, J. M.; Daniels, A. D.; Kudin, K. N.; Strain, M. C.; Farkas, O.; Tomasi, J.; Barone, V.; Cossi, M.; Cammi, R.; Mennucci, B.; Pomelli, C.; Adamo, C.; Clifford, S.; Ochterski, J.; Petersson, G. A.; Ayala, P. Y.; Cui, Q.; Morokuma, K.; Malick, D. K.; Rabuck, A. D.; Raghavachari, K.; Foresman, J. B.; Cioslowski, J.; Ortiz, J. V.; Stefanov, B. B.; Liu, G.; Liashenko, A.; Piskorz, P.; Komaromi, I.; Gomperts, R.; Martin, R. L.; Fox, D. J.; Keith, T.; Al-Laham, M. A.; Peng, C. Y.; Nanayakkara, A.; Gonzalez, C.; Challacombe, M.; Gill, P. M. W.; Johnson, B. G.; Chen, W.; Wong, M. W.; Andres, J. L.; Head-Gordon, M.; Replogle, E. S.; Pople, J. A. *Gaussian 98*, revision A.7; Gaussian, Inc.: Pittsburgh, PA, 1998.
(42) Bader, R. W. F. *Atoms in Molecules: A Quantum Theory*; Oxford University Press: Oxford, 1990.
(43) Boyd, R. J.; Choi, S. C. *Chem. Phys. Lett*. **1985**, *120*, 80.
(44) Boyd, R. J.; Choi, S. C. *Chem. Phys. Lett.* **1986**, *129*, 62.
(45) Cheeseman, J. R.; Carroll, M. T.; Bader, R. F. *W. Chem. Phys. Lett*. **1988**, *143*, 450.
(46) Carroll, M. T.; Chang, C.; Bader, R. F. W. *Mol. Phys*. **1988**, *63*, 387.
(47) Hobza, P.; Sponer, J.; Cubero, E.; Orozco, M.; Luque, F. J. *J. Phys. Chem. B* **2000**, *104*, 6286.
(48) Shishkin, O. V.; Gorb, L.; Leszczynski, J. *Int. J. Mol. Sci.* **2000**, *1*, 17.
(49) Zhanpeisov, N. U.; Zhidomirov, G. M.; Yudanov, I. V.; Klabunde, K. J. *J. Phys. Chem.* **1994**, *98*, 10032.